Mechanism and Machine Theory 164 (2021) 104401

Contents lists available at ScienceDirect

Mechanism and Machine Theory

journal homepage: www.elsevier.com/locate/mechmachtheory

Research paper

Investigation of the effect of contact pattern design on the mechanical and thermal behaviors of plastic-steel helical gear drives

Victor Roda-Casanova [a,*], Ignacio Gonzalez-Perez [b]

[a] Mechanical Engineering and Construction Department, Jaume I University, Spain
[b] Department of Mechanical Engineering, Materials and Manufacturing, Universidad Politécnica de Cartagena, Spain

ARTICLE INFO

Article history:
Received 16 April 2021
Accepted 11 May 2021

Keywords:
Polymer gears
Loaded tooth contact analysis
Frictional power loss
Thermal analysis

ABSTRACT

This article describes an investigation that has been conducted to assess the effects of the contact pattern design on the mechanical and thermal behaviors of plastic-steel helical gear drives. The maximum contact pressure, frictional power loss, transmission error function and operating temperature are determined for different designs of the pinion tooth surfaces. Several numerical examples based on loaded tooth contact analyses and steady-state heat transfer analyses are carried out considering different types of micro-geometry modifications of the involute tooth surfaces. The obtained results show that an appropriate design of the pinion tooth surfaces can help reducing the maximum contact pressure and the maximum operating temperature, increasing the durability of the transmission. The frictional power loss and the peak-to-peak transmission error can be diminished, improving the performance of the transmission and increasing its efficiency. Also, it has been shown that the design of the pinion tooth surfaces can provide some capability to the transmission to absorb angular misalignments.

© 2021 The Author(s). Published by Elsevier Ltd.
This is an open access article under the CC BY-NC-ND license
(http://creativecommons.org/licenses/by-nc-nd/4.0/)

1. Introduction

Plastic gears are replacing metallic gears in a wide range of industrial applications, as they present many advantages over their metallic counterparts: they are easy and fast to manufacture, have a reduced cost, can be used without lubricant, offer a good resistance to corrosion and bring smooth and quiet operation.

One of the main limitations of plastic gears is that their mechanical properties, and specially their load carrying capacity, are severely diminished by the increment of their working temperature [1]. Since these transmissions are usually operated without lubricant, an important amount of heat is generated by friction during the meshing of their teeth [2]. In addition, the lack of lubricant decreases the dissipation of heat. These facts, combined with the low thermal conductivity of the polymer material, accentuate the temperature rise in plastic gears.

The negative effect of the temperature increments on the durability of polymer gears is not the only concern for plastic gear designers. There are other phenomena and failure modes [3] that are often neglected in metallic gear transmissions, but

* Corresponding author.
E-mail address: vroda@uji.es (V. Roda-Casanova).

https://doi.org/10.1016/j.mechmachtheory.2021.104401
0094-114X/© 2021 The Author(s). Published by Elsevier Ltd. This is an open access article under the CC BY-NC-ND license
(http://creativecommons.org/licenses/by-nc-nd/4.0/)

play an important role in plastic gear transmissions [4]. These phenomena include an abnormal flank wear [5], an excessive tooth deformation under load [6] and a poor transmission efficiency [7] derived from frictional losses in dry running gears.

In recent times, several analytical and numerical models have been developed to predict the contact and bending stresses [8,9], the efficiency [10] and the temperature rise [11–13] of polymer gear transmissions. These advances in the simulation and analysis of polymer gears have been accompanied by new procedures for experimental tests [14–17] in which the temperature and the durability of polymer gears are assessed.

As the analysis capabilities for polymer gears increase, a range of possibilities arises during their design stages that allows their mechanical and thermal behaviors [4,16,18] to be improved. As in metallic gear transmissions, the geometry of the polymer gears can be modified in order to improve their durability and their performance under operating conditions. These modifications can be categorized into [19]:

- The macro-geometry modifications, which affect to the basic geometric parameters of the gear (module, face width, number of teeth, profile shift, pressure angle, helix angle, and type of flank curve).
- The micro-geometry modifications, which require changes to the involute tooth surface and include the tip and bottom relieves, profile and longitudinal crownings, and front and back relieves.

In the field of macro-geometry modifications for polymer gears, Walton [20] studied the effect of the tooth geometry on the efficiency of the transmission. Andrei [21] studied the influence of non-standard geometries in the sliding velocities of polymer gears. Meuleman [22] proposed methods to minimize the transmission errors in highly loaded polymer transmissions. Miler [23] and Tavčar [24] proposed optimization processes for the parameters that define the macro-geometry of polymer spur gears.

Zorko [25] showed that the substitution of an involute profile by a S-shaped flank curve can bring some advantages in the case of spur polymer gears, which include the reduction of contact stresses and a lower heat generation. Koide [26] compared the efficiency and the temperature of involute polymer gears with sine-curve polymer gears, and showed that the latter present certain advantages, especially when they are running without lubricant.

Modifications of the gear body have also been proposed to improve the thermal behavior of polymer gears. Imrek [27] proposed a tooth width modification to improve the performance of nylon 6 gears. In other approaches, cooling holes are performed in the gear blank to help decreasing the thermal damage in polymer gears [28–30]. Fernandes [31] introduced the concept of hybrid polymer gears (polymer gears with metallic inserts) to improve their thermal behavior.

A large amount of investigations dealing with macro-geometry modifications of plastic gears can be found in the literature, which contrasts with the lack of works dealing with the effects of the micro-geometry modifications over the mechanical and the thermal responses of polymer gears [19]. On the contrary, the effects of micro-geometry modifications on the mechanical behavior of metallic helical gear drives have been widely studied. Here, the number of publications is considerably higher, from the first works directed to reduce transmission errors and get quiet transmissions [32] to more recent publications [33,34] to localize the bearing contact, reduce the level of contact and bending stresses and diminish the sliding velocities.

2. Overview of the proposed investigation

In this work, the effect of different contact pattern designs on the mechanical and thermal behaviors of a plastic-steel helical gear transmission is investigated. This transmission is composed of a pinion made of AISI 1040 steel and a gear manufactured from polyoxymethylene (POM), and it is operating without lubricant. Four types of contact pattern designs are achieved through micro-geometry modifications of the pinion tooth surfaces: (i) a not-localized bearing contact as a result of no application of modifications (involute profiles), (ii) a localized bearing contact with a contact path in longitudinal direction as a result of application of profile crowning, (iii) a localized bearing contact with a contact path in profile direction as a result of application of longitudinal crowning, and (iv) a localized bearing contact in a combined direction between longitudinal and profile ones as a result of application of profile and longitudinal crownings. These designs require also the application of tip relief to avoid areas with high contact stresses.

The pinion tooth surfaces are generated by a theoretical rack-cutter of modified geometry as the one considered in [35]. The use of a theoretical modified rack-cutter allows different designs of the metallic pinion tooth surfaces to be obtained and applied in manufacturing through the use of a cutting tool.

A loaded tooth contact analysis (L-TCA) is performed by means of a finite element analysis of the transmission for each contact pattern design. The L-TCA allows the contact pressure distribution and the loaded function of transmission errors to be determined. An algorithm to determine the frictional power losses from the shear forces provided in the L-TCA is proposed. The frictional energy is computed along a cycle of meshing following the basic ideas exposed in [13] but applying them to a 3D problem. Finally, a steady-state heat transfer finite element analysis is performed to obtain the temperature distribution on the plastic gear tooth for each considered contact pattern design. The wear of the plastic gear has not been considered in this work and this may alter the observed differences between the considered types of contact pattern design, especially for high number of load cycles [17,18].

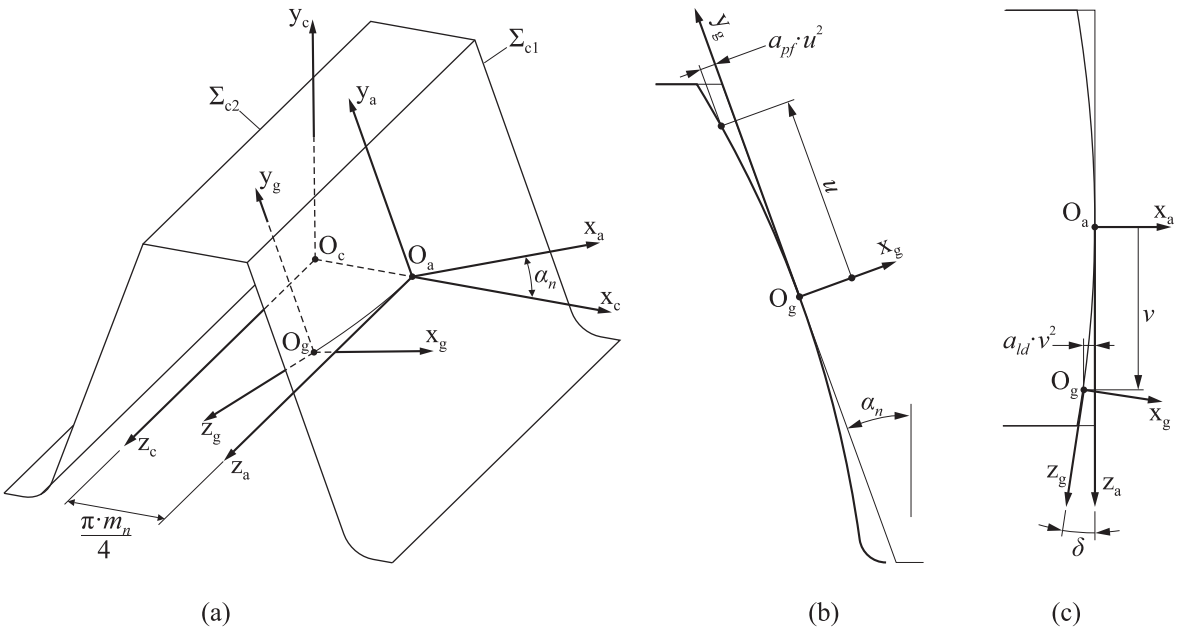

Fig. 1. For definition of the rack cutter tooth surface Σ_{c1}: (a) tooth surface, (b) illustration of profile parameter u, and (c) illustration of longitudinal parameter v.

3. Generation of pinion and gear tooth surfaces

The pinion and gear tooth surfaces are generated by an imaginary rack cutter of modified geometry as indicated in [35]. Fig. 1a shows a 3D schematic view of a rack cutter tooth, whose active tooth surfaces of driving and coast sides are denoted as Σ_{c1} and Σ_{c2}, respectively. In this figure, coordinate system S_a is rigidly connected to the rack cutter surface Σ_{c1}, and coordinate system S_c is rigidly connected to the rack cutter pitch plane (not shown in Fig. 1a).

Fig. 1 b shows the geometry of the rack cutter profile. Coordinate system S_g is an auxiliary coordinate system to take into account the profile crowning of the rack cutter tooth surface. Profile of rack cutter is represented in coordinate system S_g as:

$$\mathbf{r}_g(u) = \begin{bmatrix} -a_{pf} \cdot u^2 & u & 0 & 1 \end{bmatrix}^T \tag{1}$$

where u is the surface parameter in profile direction and a_{pf} is a parabola coefficient. By setting $a_{pf} = 0$, a straight profile is achieved.

Surface Σ_{c1} is represented in coordinate system S_a as:

$$\mathbf{r}_a(u, v) = \mathbf{M}_{ag}(v) \cdot \mathbf{r}_g(u) \tag{2}$$

where $\mathbf{M}_{ag}(v)$ is the transformation matrix from coordinate system S_g to coordinate system S_a (see Fig. 1c):

$$\mathbf{M}_{ag}(v) = \begin{bmatrix} \cos\delta & 0 & -\sin\delta & -a_{ld} \cdot v^2 \\ 0 & 1 & 0 & 0 \\ \sin\delta & 0 & \cos\delta & v \\ 0 & 0 & 0 & 1 \end{bmatrix} \tag{3}$$

Here, v is the other surface parameter, a_{ld} is the parabola coefficient for the longitudinal crowning of the rack cutter tooth surface, and angle δ can be calculated as $\delta = \text{atan}(2 \cdot a_{ld} \cdot v)$.

Rack cutter generating surface can be represented in coordinate system S_c as:

$$\mathbf{r}_c(u, v) = \mathbf{M}_{ca} \cdot \mathbf{r}_a(u, v) \tag{4}$$

where $\mathbf{M}_{ca}$ is the transformation matrix from coordinate system S_a to coordinate system S_c:

$$\mathbf{M}_{ca} = \begin{bmatrix} \cos\alpha_n & -\sin\alpha_n & 0 & \frac{\pi \cdot m_n}{4} \\ \sin\alpha_n & \cos\alpha_n & 0 & 0 \\ 0 & 0 & 1 & 0 \\ 0 & 0 & 0 & 1 \end{bmatrix} \tag{5}$$

Here, α_n is the normal pressure angle and m_n is the normal modulus of the helical gear drive. Only the equations to determine the rack cutter tooth surface Σ_{c1} have been presented for the purpose of simplicity.

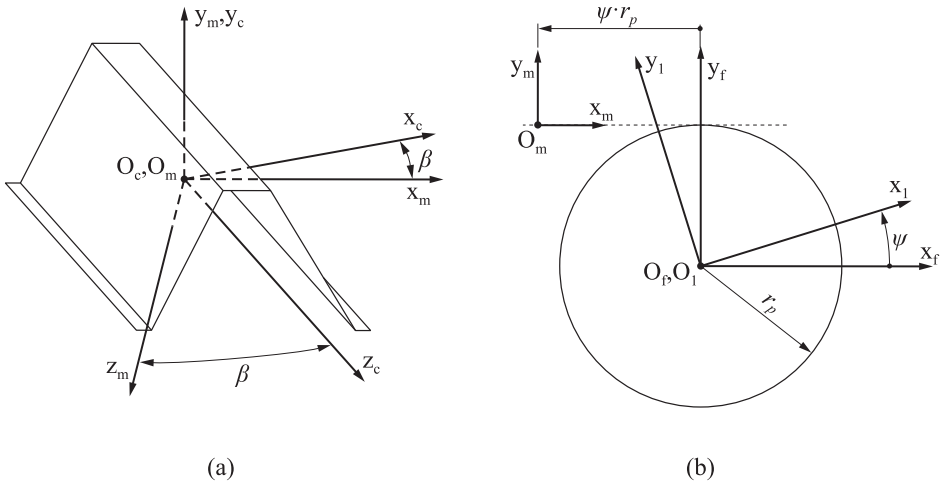

Fig. 2. For derivation of pinion tooth surface.

Coordinate transformation from system S_c to system S_1 (see Fig. 2) and observation of the equation of meshing allows the pinion tooth surface to be determined from the rack-cutter tooth surface:

$$\mathbf{r}_1(u, v, \psi) = \mathbf{M}_{1m}(\psi) \cdot \mathbf{M}_{mc} \cdot \mathbf{r}_c(u, v) \tag{6}$$

$$\left(\frac{\partial \mathbf{r}_1}{\partial u} \times \frac{\partial \mathbf{r}_1}{\partial v}\right) \cdot \frac{\partial \mathbf{r}_1}{\partial \psi} = 0 \tag{7}$$

Here, ψ is the generalized parameter of generation and matrixes $\mathbf{M}_{mc}$ and $\mathbf{M}_{1m}$ are given by:

$$\mathbf{M}_{mc} = \begin{bmatrix} \cos\beta & 0 & \pm\sin\beta & 0 \\ 0 & 1 & 0 & 0 \\ \mp\sin\beta & 0 & \cos\beta & 0 \\ 0 & 0 & 0 & 1 \end{bmatrix} \tag{8}$$

$$\mathbf{M}_{1m} = \begin{bmatrix} \cos\psi & \sin\psi & 0 & 0 \\ -\sin\psi & \cos\psi & 0 & 0 \\ 0 & 0 & 1 & 0 \\ 0 & 0 & 0 & 1 \end{bmatrix} \cdot \begin{bmatrix} 1 & 0 & 0 & -\psi \cdot r_p \\ 0 & 1 & 0 & r_p \\ 0 & 0 & 1 & 0 \\ 0 & 0 & 0 & 1 \end{bmatrix} \tag{9}$$

where β is the helix angle and r_p is the pinion pitch radius. The upper sign in matrix $\mathbf{M}_{mc}$ is applied to a left hand gear and the lower sign is applied to a right hand gear.

3.1. Tip relief

Tip relief of the gear tooth surfaces is required to release the tip from high values of contact pressures. Fig. 3 describes the geometry of the tip relief. In this figure, S_b is an auxiliary coordinate system that is rigidly connected to coordinate system S_g.

The origin of S_b is defined by point O_b, which is located on the profile at a distance $u_{0_{top}}$ from O_g, and defines the lower limit of the tip relief. The lower limit of the tip relief can also be defined by distance $h_{0_{top}}$ from the tip of the profile, as indicated in Fig. 3b. Coordinate system S_b is rotated an angle $\gamma = \text{atan}\left(2 \cdot a_{pf} \cdot u_{0_{top}}\right)$ with respect to S_g, as indicated in Fig. 3a.

The tip relief of rack cutter is represented in coordinate system S_b as:

$$\mathbf{r}_b(u) = \left[-a_{pf_{top}} \cdot \left(\frac{u - u_{0_{top}}}{\cos\gamma}\right)^2 \quad \frac{u - u_{0_{top}}}{\cos\gamma} \quad 0 \quad 1\right]^T \tag{10}$$

where $a_{pf_{top}}$ is the parabola coefficient for the tip relief. If a straight tip relief is desired, then $a_{pf_{top}}$ is set to 0.

The tip relief is represented in coordinate system S_g as:

$$\mathbf{r}_g(u) = \mathbf{M}_{gb} \cdot \mathbf{r}_b(u) \tag{11}$$

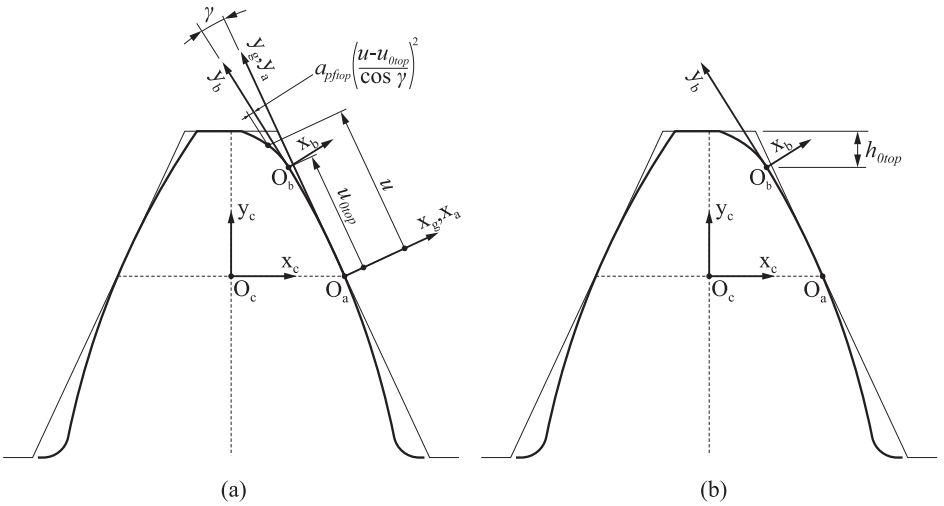

Fig. 3. For definition of tip relief: (a) geometry of the rack cutter profile, (b) illustration of $h_{0_{top}}$.

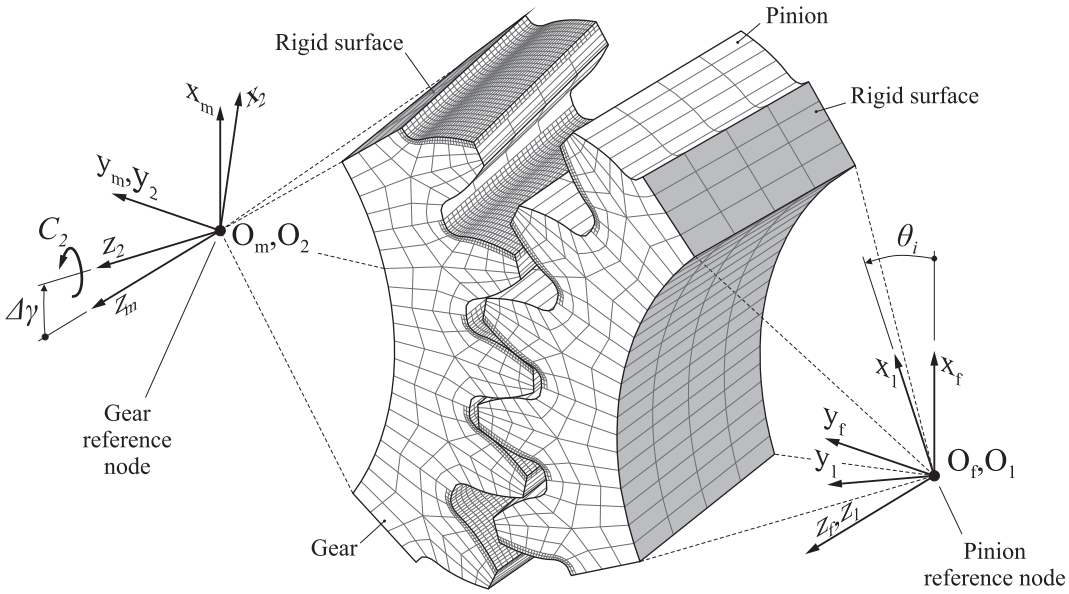

Fig. 4. Description of the finite element model for L-TCA.

where $\mathbf{M}_{gb}$ is a transformation matrix from S_b to S_g and it is defined as:

$$\mathbf{M}_{gb} = \begin{bmatrix} \cos\gamma & -\sin\gamma & 0 & -a_{pf} \cdot u_{0_{top}}^2 \\ \sin\gamma & \cos\gamma & 0 & u_{0_{top}} \\ 0 & 0 & 1 & 0 \\ 0 & 0 & 0 & 1 \end{bmatrix} \tag{12}$$

4. Loaded tooth contact analysis of the gear transmission

The loaded tooth contact analysis of the transmission under investigation is performed through a set of static finite element analyses using the 3D finite element model illustrated in Fig. 4. Here, a reduced number of elements is illustrated for the purpose of simplicity. The basis for the construction of the finite element mesh can be found in [36] where two independent meshes are tied through a surface constraint. Fig. 4 shows a fixed coordinate system S_f where pinion and gear models are assembled. An auxiliary coordinate system S_m is defined parallel to S_f and remains as well fixed during the analyses. The origin of coordinate system S_m is located on axis y_f at a distance from O_f that coincides with the center distance of the transmission.

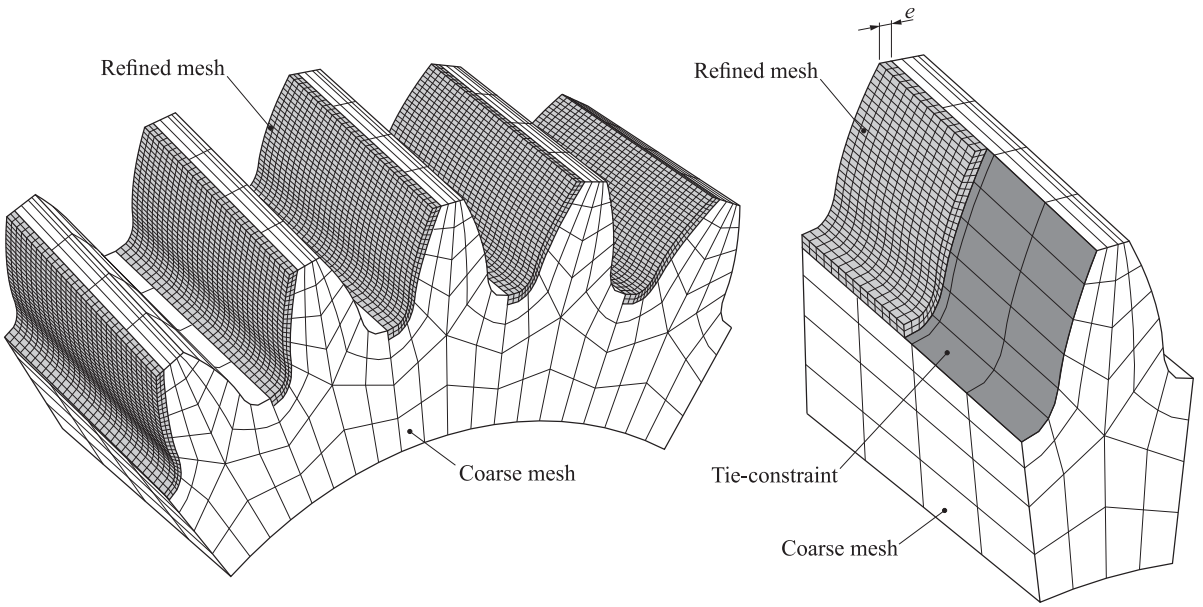

Fig. 5. Schematic representation of the finite element mesh.

Pinion and gear models consist of five teeth and are defined in coordinate systems S_1 and S_2 (see Fig. 4), respectively. Nodes located on both sides and bottom part of the corresponding rims form rigid surfaces. A pinion reference node (respectively, a gear reference node) is defined at the origin of system S_1 (respectively, system S_2) and is rigidly connected to its corresponding rigid surface, allowing a rigid body motion between the reference node and its rigid surface. Rotation of the pinion is considered through angle θ_i by releasing the degree of freedom of the pinion reference node about axis z_f and blocking it at each frame of the analysis. Assembling of system S_2 in auxiliary coordinate system S_m may be accompanied by a shaft angle error $\Delta\gamma$ about axis y_m. A torque C_2 is applied through the released degree of freedom of the gear reference node represented by the rotation about axis z_2.

Fig. 5 shows a more detailed view of the two independent meshes: (i) a refined mesh composed by several layers of first order hexahedral elements (reference C3D8I in [37]) and characterized by thickness e (two layers for the purpose of simplicity are represented in Fig. 5), and (ii) a coarse mesh composed of second order hexahedral elements (reference C3D20 in [37]). A tie-surface constraint between these two independent meshes is established to guarantee the continuity of displacements all over the gear models (see details in [36]).

Surface-to-surface finite sliding contact pairs are specified between the teeth of both gears. A penalty method is established to take into account the tangential behavior of the contact, where a constant or a variable coefficient of friction can be specified. A linear elastic material is defined for the elements of both gear geometries, under the assumption that the deformations are so small that can be studied under the assumptions of the small strain theory.

The static analysis is repeated for several contact positions distributed along the cycle of meshing of the central pair of teeth, from the initial to the final contact positions of such an engagement. Each contact position i is characterized by a value of the angle θ_i (Fig. 4), which varies between θ_{ini} (which defines the initial contact position) and θ_{end} (which defines the final contact position). The analyzed contact positions form an increasing sequence in which $\theta_i < \theta_{i+1}$. Each analyzed contact position has an associated time t_i which, assuming that the transmission under study is operating at a constant angular velocity ω_1, can be calculated as:

$$t_i = t_{ini} + \frac{\theta_i - \theta_{ini}}{\omega_1} \tag{13}$$

where $t_{ini} = 0\ s$ is the time instant associated to the initial contact position.

For each contact position, results such as the maximum contact pressure can be directly retrieved from the finite element solver. The procedures to obtain derived results such as the loaded transmission error or the frictional power loss are discussed in sections 4.1 and 4.2, respectively.

Compared to other approaches based on analytical methods, this approach has the advantage of taking into account the effects derived from the elastic deformations of the gear teeth, such as variations in the gear kinematics [38], changes in the contact ratio [9] and modifications of the load sharing between teeth [39].

4.1. Determination of loaded transmission errors

The vectors that describe the angular velocity and angular position of the pinion are, respectively:

$$\boldsymbol{\omega}_{R1,i} = [0, 0, \omega_1] \tag{14}$$

$$\boldsymbol{\theta}_{R1,i} = [0, 0, \theta_i] \tag{15}$$

After conducting L-TCA, vector $\boldsymbol{\theta}_{R2,i}$, that describes the angular rotation of the reference node of the gear, can be retrieved for each contact position i. Then, vector $\boldsymbol{\omega}_{R2,i}$, that represents the angular velocity of the gear, is calculated using a finite difference differentiation scheme:

$$\boldsymbol{\omega}_{R2,i} = \frac{\boldsymbol{\theta}_{R2,i+1} - \boldsymbol{\theta}_{R2,i-1}}{t_{i+1} - t_{i-1}} \tag{16}$$

The magnitude of the transmission error $\Delta\phi_i$ can be obtained as:

$$\Delta\phi_i = |\boldsymbol{\theta}_{R2,i} - \boldsymbol{\theta}_{R2,ini}| - \frac{z_1}{z_2} \cdot |\boldsymbol{\theta}_{R1,i} - \boldsymbol{\theta}_{R1,ini}| \tag{17}$$

Here, z_1 and z_2 are the pinion and gear tooth numbers, respectively. The peak-to-peak value of transmission error is then obtained as:

$$\Delta\phi_{ptp} = \max \Delta\phi_i - \min \Delta\phi_i \tag{18}$$

4.2. Determination of frictional power losses

During the meshing of the gears, there is a certain amount of power that is lost due to the sliding between the contacting surfaces. This frictional power loss causes a decrease of the efficiency of the transmission and an undesired temperature increase of the gears, since a part of this frictional power is converted into heat.

From the results of the L-TCA, a frictional power dissipation value can be determined for each contact position i at each node j of the contacting surfaces of the gear. For such a purpose:

1. Retrieve the deformed position $\mathbf{u}_{j,i}$ and the tangential contact force $\mathbf{F}_{Tj,i}$.
2. For those nodes where $\left|\mathbf{F}_{Tj,i}\right| > 0$ compute the instantaneous sliding velocity $\mathbf{v}_{Sj,i}$ as:

$$\mathbf{v}_{Sj,i} = \boldsymbol{\omega}_{R2,i} \times \left(\mathbf{u}_{j,i} - \overrightarrow{O1O2}\right) - \boldsymbol{\omega}_{R1,i} \times \mathbf{u}_{j,i} \tag{19}$$

   where $\overrightarrow{O1O2}$ is a vector that defines the position of point O_2 with respect to point O_1 (see Fig. 4). Vector $\overrightarrow{O1O2}$ does not change during the simulation. For those cases where $\left|\mathbf{F}_{Tj,i}\right| = 0$ the sliding velocity $\mathbf{v}_{Sj,i}$ is set to zero.
3. Compute the nodal frictional power dissipation as:

$$H_{j,i} = \mathbf{v}_{Sj,i} \cdot \mathbf{F}_{Tj,i} \tag{20}$$

Once the previous steps are completed, the instantaneous frictional power loss of the gear transmission at contact position i is calculated as the sum of all the nodal contributions:

$$\hat{H}_i = \sum_{j=1}^{n_n} H_{j,i} \tag{21}$$

where n_n is the number of nodes in the contacting surfaces of the gear. The frictional energy dissipated at each node j during the cycle of meshing can be calculated using the trapezoidal integration rule, assuming linear interpolation of the nodal frictional power in the time domain:

$$E_j = \sum_{i=1}^{n_c-1} \frac{\left(H_{j,i} + H_{j,i+1}\right) \cdot (t_{i+1} - t_i)}{2} \tag{22}$$

where n_c is the number of contact positions in which the analysis is performed.

Finally, the average frictional power dissipation of the transmission can be calculated as:

$$\bar{H} = \frac{\omega_1}{\theta_{end} - \theta_{ini}} \cdot \sum_{j=1}^{n_n} E_j \tag{23}$$

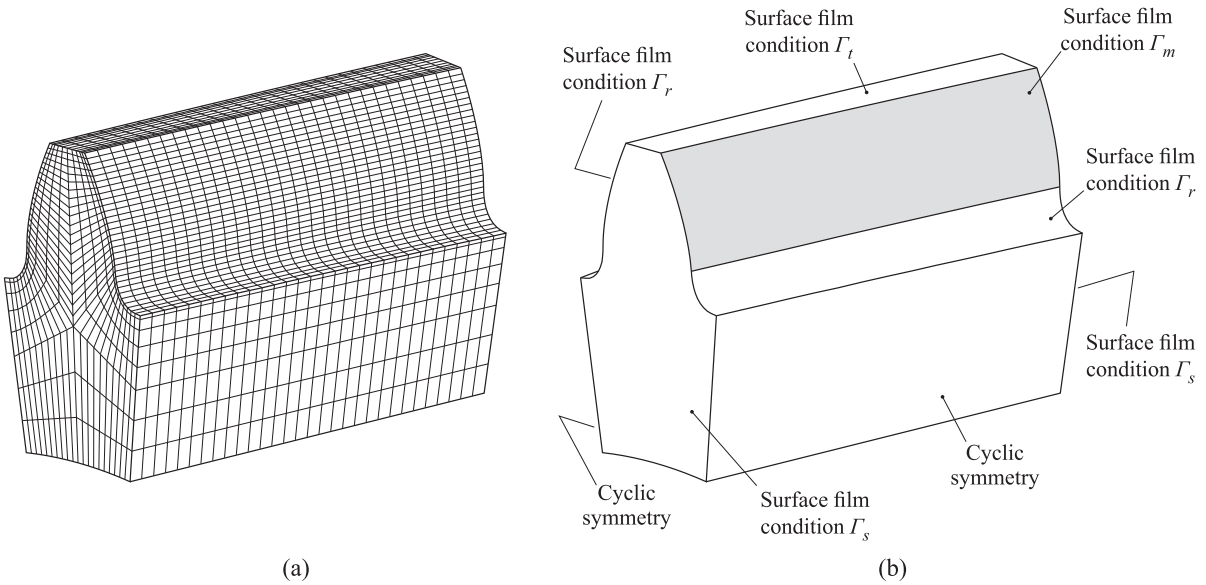

Fig. 6. Finite element model applied in the thermal analysis: (a) finite element mesh and (b) boundary conditions.

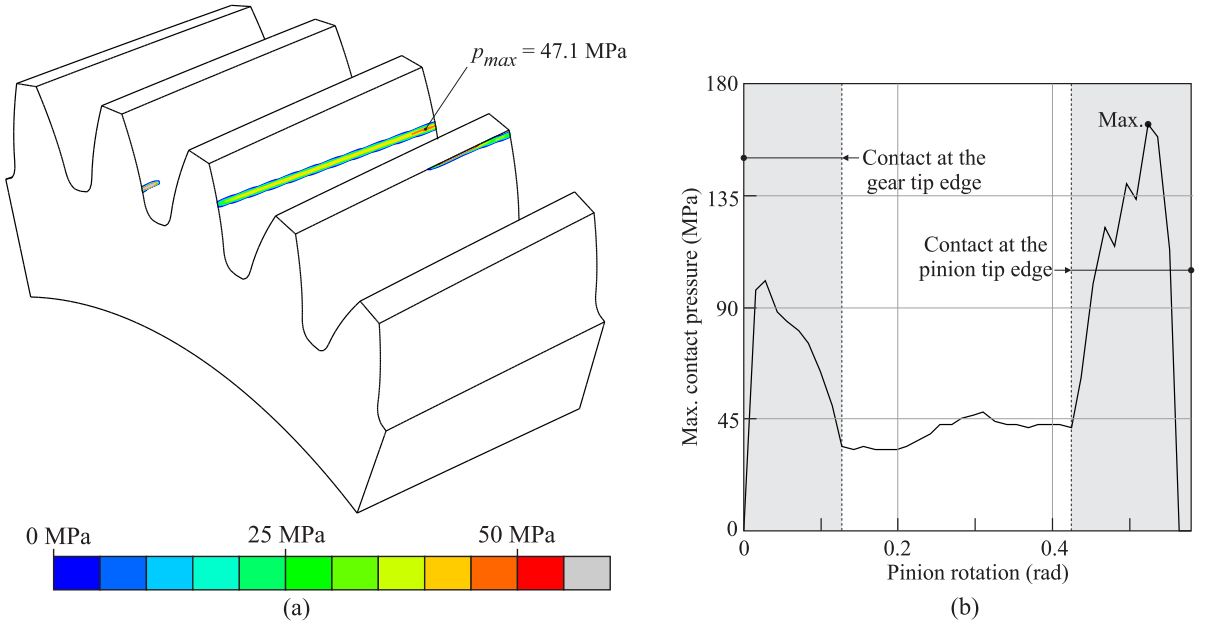

Fig. 7. Results of analyses for case CS00: (a) contact pressure distribution and (b) evolution of the maximum contact pressure at the central tooth of the gear.

5. Determination of the operating temperature of the gear through a thermal finite element analysis

The thermal performance of the transmission is assessed through a steady-state heat transfer analysis of a finite element model of one gear tooth, as the one shown in Fig 6. This model is discretized into linear finite elements (reference DC3D8 in [37]) following the ideas described in [40]. A cyclic symmetry is considered as a boundary condition at both sides of the tooth rim (Fig 6 b) where a tooth is joined with its adjacent teeth.

The thermal loads considered in this finite element analysis are derived from the L-TCA as described in Section 5.2. To ensure the compatibility of these thermal loads with the finite element mesh, the position of the nodes on the active flank of the considered tooth must coincide with the position of the nodes on the active flank of the finite element model used for the L-TCA (described in Section 4). This requirement only applies to the nodes on the active flank; the rest of the nodes

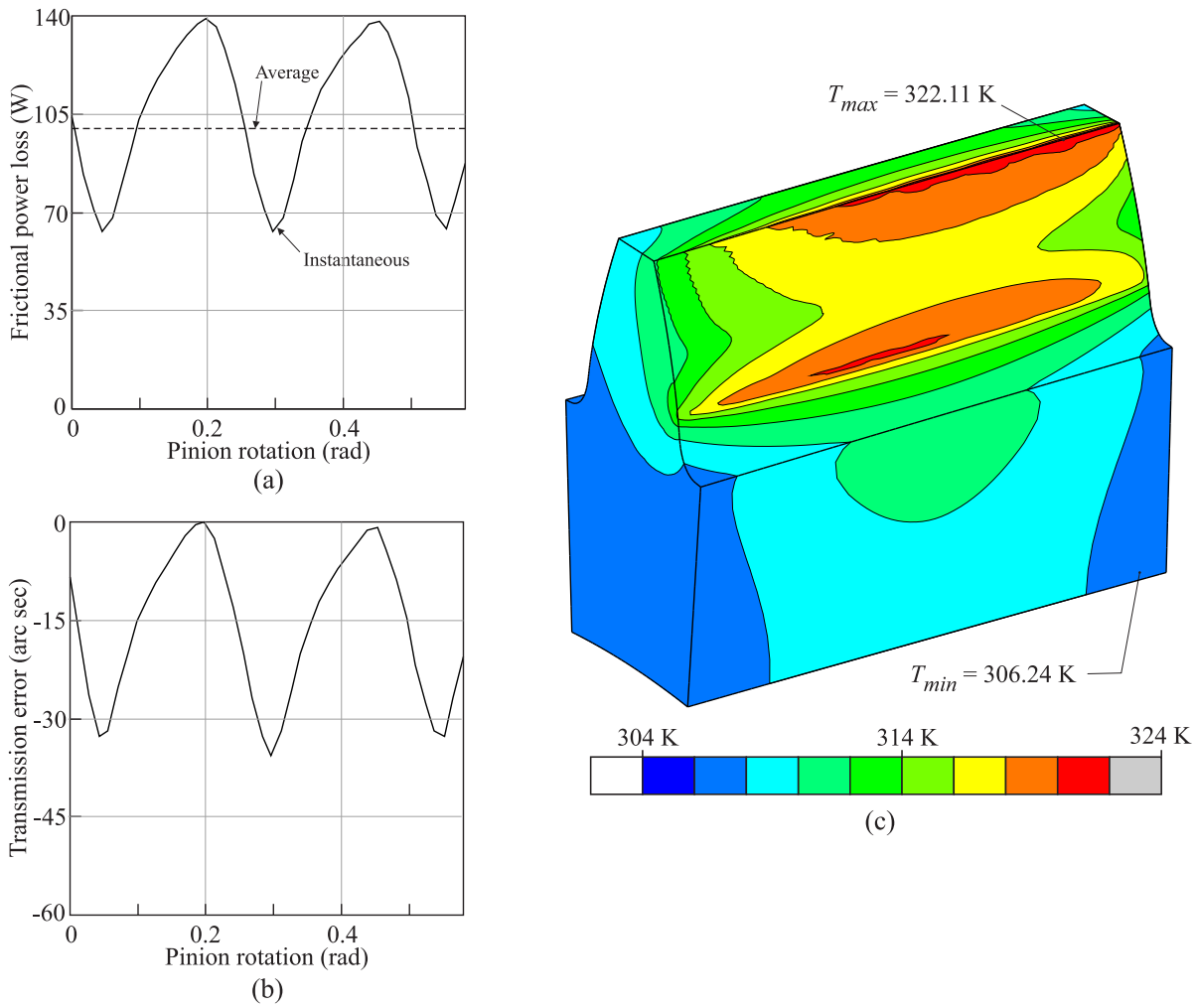

Fig. 8. Results of analyses for case CS00: (a) instantaneous power loss, (b) loaded function of transmission errors and (c) temperature distribution.

in the mesh can be set at any arbitrary position. Additionally, element DC3D8 assures compatibility with the derived heat fluxes at the nodes of elements C3D8I.

Of the three heat transfer mechanisms, only conduction and convection are considered in the proposed finite element model. Radiation is not taken into account because it is assumed that the amount of heat dissipated by radiation is small compared to the heat dissipated by the other heat transfer mechanisms.

In steady-state conditions, heat conduction is characterized by the thermal conductivity of the gear material. Heat convection is modeled through four surface film conditions (denoted by Γ_m, Γ_r, Γ_s and Γ_t) that are applied to the external surfaces of the gear, as shown in Fig. 6b. Surface film condition Γ_s is specified for the front and back sides of the tooth, Γ_t is specified for the top land, Γ_r is specified for the non-meshing flank and the fillet of the meshing flank, and Γ_m is specified for the active part of the meshing flank. Each surface film condition is characterized by the environment temperature T_{env} and a heat transfer coefficient (h_s, h_t, h_r and h_m, respectively) whose calculation method is described in Section 5.1.

After the analysis of this finite element model, the temperature field across the geometry of the gear tooth is obtained.

5.1. Convective heat transfer coefficients

The convective heat transfer coefficients play a major role in the simulation of the convective cooling of gears. Different approaches can be found in the literature for the calculation of these coefficients [11,12,41–43] and, among them, the one proposed by Fernandes [12] has been followed in this work.

In this approach, the selection of the calculation method for the heat transfer coefficient h_s (surface film condition Γ_s) depends on the type of flow that is produced at the sides of the gear (laminar, turbulent or transition flow). Assuming that

the air flow at these parts of the gear is laminar, the heat transfer coefficient h_s can be calculated as [44]:

$$h_s = 0.308 \cdot (m_h + 2)^{0.5} \cdot Pr_{air}^{0.5} \cdot k_{air} \cdot \sqrt{\frac{\omega}{\nu_{air}}} \tag{24}$$

where k_{air}, ν_{air} and Pr_{air} are the thermal conductivity, the kinematic viscosity and the Prandtl number, respectively, of the surrounding air. Moreover, ω is the angular velocity of the gear and $m_h = 2$ is the exponent of the assumed power function wall temperature distribution that is used for the derivation of Eq. 24 (see [43]).

Heat transfer coefficient h_t (surface film condition Γ_t) is assumed to be equal to the maximum value of the heat transfer determined for surface film condition Γ_s:

$$h_t = \max(h_s) \tag{25}$$

The heat transfer coefficient h_r (surface film condition Γ_r) is assumed to be comprised between $\frac{1}{2}$ and $\frac{1}{3}$ of the heat transfer specified for surface film condition Γ_s:

$$\frac{h_s}{3} \leq h_r \leq \frac{h_s}{2} \tag{26}$$

Finally, two different heat transfer coefficients ($h_m^{(1)}$ and $h_m^{(2)}$) are considered for surface film condition Γ_m, and its election depends on whether the considered tooth is assumed to be engaged or not:

- When the tooth is not engaged, the heat transfer coefficient $h_m^{(1)}$ is the same as for the non-meshing flank ($h_m^{(1)} = h_r$).
- When the tooth is engaged, the heat transfer coefficient $h_m^{(2)}$ can be determined as suggested by Handschuh [45]:

$$h_m^{(2)} = 0.228 \cdot \left(\frac{r^2 \cdot \omega}{\nu_{air}}\right)^{0.731} \cdot Pr_{air}^{1/3} \cdot \frac{k_{air}}{d} \tag{27}$$

where d is the reference diameter of the gear and r is the distance between any meshing point and the axis of rotation of the gear.

For the steady-state analysis the heat transfer coefficient for surface film condition Γ_m must be time-independent and, following the ideas presented in [12], a time-averaged heat transfer coefficient is calculated as:

$$h_m^{'} = \frac{h_m^{(2)}}{z} + \left(1 - \frac{1}{z}\right) \cdot h_m^{(1)} \tag{28}$$

5.2. Thermal loads

In plastic-steel gear transmissions, heat is mainly originated from two different sources: (i) dissipation of the frictional energy that is produced at the contact between teeth, and (ii) dissipation of the hysteresis energy caused by the deformation of the gear viscoelastic material. In the great majority of the thermal analysis the latter is neglected, since it has been demonstrated [2] that its contribution to the increase of the temperature of the gears is small compared to the contribution of the frictional heating. Thus, only the thermal loads derived from the heat flux generated by friction are considered in the heat transfer analysis.

Following the results obtained from the L-TCA of the transmission, the heat flux on a given node k of the contacting surface of the gear central tooth, at each contact position i, can be calculated as (see [12,13,43]):

$$q_{k,i} = \lambda \cdot H_{k,i} \cdot \varphi_{k,i} \tag{29}$$

where λ is a constant that represents the amount of frictional power that is turned into heat and $\varphi_{k,i}$ is a heat partition factor for the distribution of this heat between the interacting surfaces. Here, subindex k just covers the nodes of the contacting surface of the gear central tooth. Assuming that the contact between gear tooth surfaces is a particular type of band contact, heat can be partitioned following Blok's equation [46]:

$$\varphi_{k,i} = \frac{\sqrt{\nu_{T2k,i}} \cdot \varepsilon_2}{\sqrt{\nu_{T1k,i}} \cdot \varepsilon_1 + \sqrt{\nu_{T2k,i}} \cdot \varepsilon_2} \tag{30}$$

In the previous equation, ε_1 and ε_2 are the thermal effusivities of the pinion and gear, respectively. On the other hand, $\nu_{T1k,i}$ and $\nu_{T2k,i}$ can be calculated from the results of the L-TCA as:

$$\nu_{T1k,i} = \left[\boldsymbol{\omega}_{R1,i} \times \mathbf{u}_{k,i}\right] \cdot \frac{\mathbf{v}_{Sk,i}}{|\mathbf{v}_{Sk,i}|} \tag{31}$$

$$\nu_{T2k,i} = \left[\boldsymbol{\omega}_{R2,i} \times \left(\mathbf{u}_{k,i} - \overrightarrow{O1O2}\right)\right] \cdot \frac{\mathbf{v}_{Sk,i}}{|\mathbf{v}_{Sk,i}|} \tag{32}$$

As it has been mentioned before, in a steady-state analysis all the variables that define the finite element model must be time-independent, including the nodal fluxes. In contrast, the nodal flux given by Eq. 29 is time-dependent, since its

Table 1
Design parameters and operating conditions of the helical transmission.

Parameter	Values
Normal modulus, m_n	3 mm
Normal pressure angle, α_n	20 deg
Helix angle, β	10 deg
Pinion helix hand	Right
Face width, b	20 mm
Pinion tooth number, z_1	25
Gear tooth number, z_2	40
Input velocity, ω_1	2500 rpm
Output torque, C_2	19.2 N m
Ambient temperature, T_{env}	302.15 K

Table 2
Definition of the three sets of cases of study.

Parameter	Set A	Set B	Set C
a_{pf} (μm^{-1})	0, 1, 3, 5, 7	0	0, 1, 3, 5, 7
a_{ld} (μm^{-1})	0	0, 0.1, 0.2, 0.3	0.1
$a_{pf_{top}}$ (μm^{-1})	0, 15, 30, 45	0, 15, 30, 45	0, 15, 30, 45
$h_{0_{top}}$ (mm)	1.2	1.2	1.2
Total cases of study	20	16	20

Table 3
Definition of selected cases of study.

Name	CS00	CS01	CS02	CS03	CS04
a_{pf} (μm^{-1})	0	0	3	0	3
a_{ld} (μm^{-1})	0	0	0	0.1	0.1
$a_{pf_{top}}$ (μm^{-1})	0	30	30	30	30
$h_{0_{top}}$ (mm)	0	1.2	1.2	1.2	1.2

magnitude changes from one to another contact position. For this reason, an averaged nodal heat flux $\bar{q}_k$ must be derived that, being constant in time, releases at each node the same amount of thermal energy as the original nodal heat flux. This averaged nodal heat flux is calculated as:

$$\bar{q}_k = \frac{\omega_2}{2\pi \text{ rad}} \cdot \sum_{i=1}^{n_c-1} \frac{\left(q_{k,i} + q_{k,i+1}\right) \cdot (t_{i+1} - t_i)}{2} \tag{33}$$

6. Definition of cases of study

This investigation is performed considering a helical gear transmission whose macro geometry design parameters and operating conditions are shown in Table 1. The variables of this study are the design parameters of the pinion tooth surfaces:

- Parabola coefficient for the profile crowning, a_{pf}.
- Parabola coefficient for the longitudinal crowning, a_{ld}.
- Parabola coefficient for the tip relief, $a_{pf_{top}}$.
- Distance for the tip relief, $h_{0_{top}}$.

A case of study is defined by assigning a value to each one of these design variables. In case that tip relief is applied to the pinion, it is also applied to the gear with the same values of $a_{pf_{top}}$ and $h_{0_{top}}$. In this work, the following studies have been performed by using the three sets of cases described in Tab. 2 (providing a total of 56 cases of study):

- Set A to study the effect of having a localized bearing contact with a contact path in longitudinal direction.
- Set B to study the effect of having a localized bearing contact with a contact path in profile direction.
- Set C to study the effect of having a localized bearing contact with a contact path in a combined direction.

Finally, five different cases of study that are representative for each type of contact pattern design have been selected for comparison purposes. Their design variables are shown in Tab. 3. These selected cases of study comprise an involute tooth surface (CS00), an involute tooth surface with tip relief (CS1), a profile crowned tooth surface with tip relief (CS2), a longitudinal crowned tooth surface with tip relief (CS3) and a double-crowned tooth surface with tip relief (CS4).

Table 4
Mechanical and thermal properties of the gear materials [4,47,48].

Property	Steel	POM
Young's modulus, E	206 GPa	2.69 GPa*
Poisson coefficient, υ	0.30	0.44
Limiting flank stress, σ_{Hlim}	-	60 MPa**
Friction coefficient, μ	0.2	
Density, ρ	7850 $\frac{kg}{m^3}$	1410 $\frac{kg}{m^3}$
Thermal conductivity, k	52 $\frac{W}{m \cdot K}$	0.3 $\frac{W}{m \cdot K}$
Specific heat, cp	470 $\frac{J}{kg \cdot K}$	1470 $\frac{J}{kg \cdot K}$

*Valid for 30°C according to [48]
**Valid for 10^6 cycles at 40°C according to [47]

Table 5
Thermal properties of the surrounding air at 300 K.

Property	Magnitude
Thermal conductivity, k_{air}	$2.624 \cdot 10^{-2}$ $\frac{W}{m \cdot K}$
Prandtl number, Pr_{air}	0.707
Kinematic viscosity, ν_{air}	$1.568 \cdot 10^{-5}$ $\frac{m^2}{s}$

7. Results and discussion

For each case of study, a L-TCA is conducted following the indications given in Section 4. The mechanical and thermal properties considered for the pinion and gear materials are shown in Table 4. A limiting flank stress of 60 MPa in the plastic material is considered since it guarantees 10^6 cycles when the gears are operating at 40°C [47].

The generated finite element models have 232,352 nodes and 174,300 elements, and they have been analyzed in 42 contact positions along the engagement of a pair of teeth. The refined mesh for the active flanks consist of four layers of elements and its total thickness is $e = 0.15 \cdot m_n$, where m_n is the normal module of the transmission (Fig. 5b). The refined mesh of the pinion has 59 elements in profile direction and 65 elements in longitudinal direction, whereas the refined mesh of the gear has 64 elements in profile direction and 75 elements in longitudinal direction.

For each case of study, the operating temperature of the gear is assessed through a steady-state heat transfer analysis, which is conducted following the indications given in Section 5. The resulting finite element model has 76304 nodes and 68100 elements. For the calculation of the convective heat transfer coefficients, the thermal properties of the surrounding air are considered, which are shown in Table 5. The thermal loads have been derived from the results of the L-TCA considering $\lambda = 1$, which indicates that all the frictional energy is dissipated as heat.

In the following sections the effect of different contact pattern designs on the mechanical and thermal behaviors of the helical transmission is analyzed.

7.1. Not-localized bearing contact

In this section, the mechanical and thermal behaviors of a helical gear transmission with involute profiles (case of study CS00 in Tab. 3) are analyzed. Fig. 7a shows the contact pressure distribution on the gear model at certain contact position of the cycle of meshing. It is observed that contact occurs simultaneously in three teeth. At the central tooth, the maximum contact pressure is 47.1 MPa.

The evolution of the maximum contact pressure at the central tooth during one cycle of meshing is shown in Fig. 7b. As it can be observed, the contact pressure reaches a local maximum at the beginning of the cycle of meshing, when the contact occurs at the gear tip edge. When the gear tooth tip is no longer in contact, the maximum contact pressure rapidly decreases to 45 *MPa*, and increases again as the contact tends towards the pinion tip edge, where the global maximum contact pressure is found (164 *MPa*). Such an elevated contact pressure produces contact stresses that exceed the yield point of the material (which is established between 60 and 75MP for POM according to Ref[48].), and this could lead to unrealistic stress results in those regions where the assumptions of the linear elastic material are not fulfilled.

Fig. 8 a shows the evolution of the instantaneous frictional power loss, which fluctuates between a minimum value of 63 W (when the contact is produced in the vicinity of the pitch circle) and a maximum value of 139 W. The average value of the frictional power loss, which is also displayed in the figure, is 102.9 W. Fig. 8b shows the loaded function of transmission errors for this case of study, where the peak-to-peak transmission error is 35.8 *arc* sec.

Finally, Fig. 8c shows the temperature distribution obtained from the thermal analysis of the gear. The maximum temperature is 322.11 K, and this represents a maximum temperature increment of 19.96 K with respect to the ambient temperature.

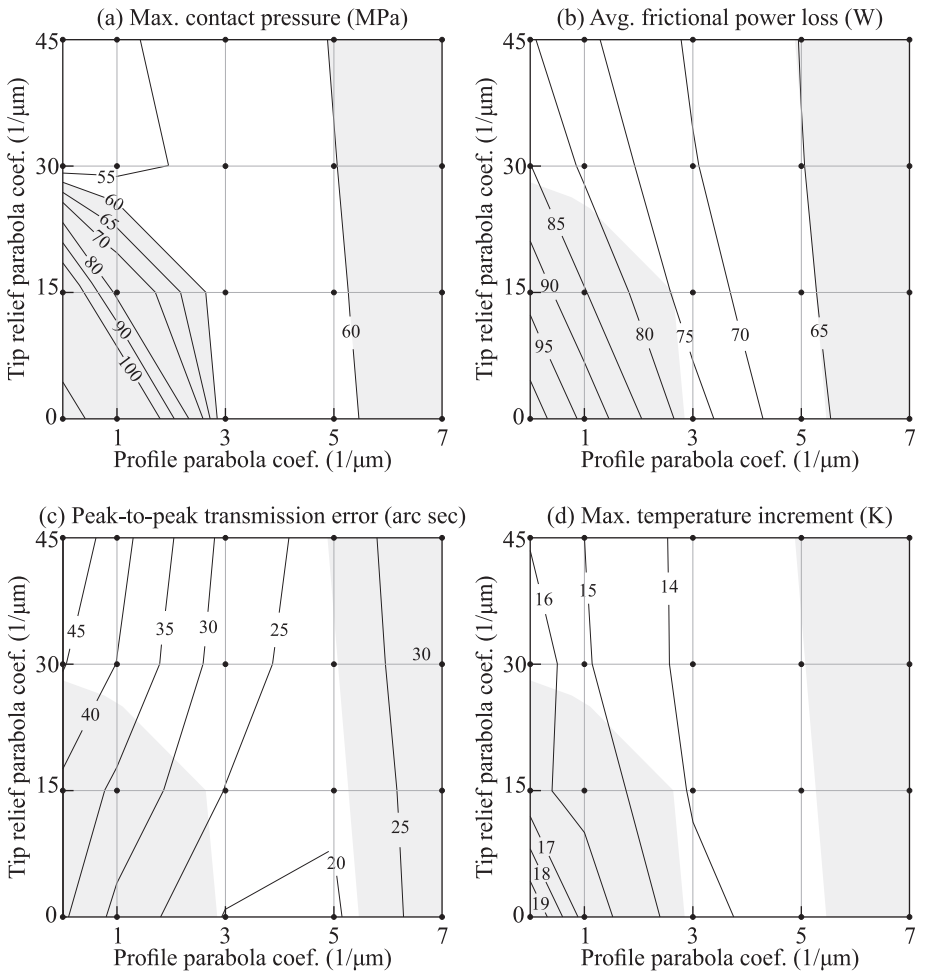

Fig. 9. Results for set A of cases.

7.2. Localized bearing contact with a contact path in longitudinal direction

Fig. 9 shows the results obtained from different combinations of profile crowning and tip relief (set A of cases in Table 2). The black dots indicate those combinations that have been studied, and the isolines are interpolated from the results of the studied cases.

Fig. 9 a shows the maximum contact pressure that is produced during the engagement of the central pair of teeth. The area shaded in grey (which is also reproduced in Figs. 9b, c and d), indicates those combinations of profile crowning and tip relief that lead to maximum contact pressures above 60 *MPa* (considered as the admissible contact pressure for the plastic material), which are produced as a consequence of a tip contact. When the contact at the tip is avoided (because of the tip relief, the profile crowning or a combination of both) the maximum contact pressures descent rapidly to values below 65 *MPa*.

Fig. 9 b shows the average frictional power loss that is produced during the meshing of the gears. It decreases as the parabola coefficient for the tip relief is increased, because the areas where the sliding velocity reaches its maximum values are removed. This behavior has already been reported in previous investigations [49]. Besides that, the average frictional power loss also decreases as the parabola coefficient for the profile crowning is increased. An explanation can be found in a narrower contact pattern around the pitch circle.

Fig. 9 c shows the peak-to-peak transmission error. For any parabola coefficient of the profile crowning below $a_{pf} = 6.0\ \mu m^{-1}$, the tip relief produces an increase of the peak-to-peak transmission error. On the other hand, the peak-to-peak transmission error tends to decrease as the parabola coefficient of the profile crowning is increased, until a minimum is found between $a_{pf} = 3\ \mu m^{-1}$ and $a_{pf} = 5\ \mu m^{-1}$.

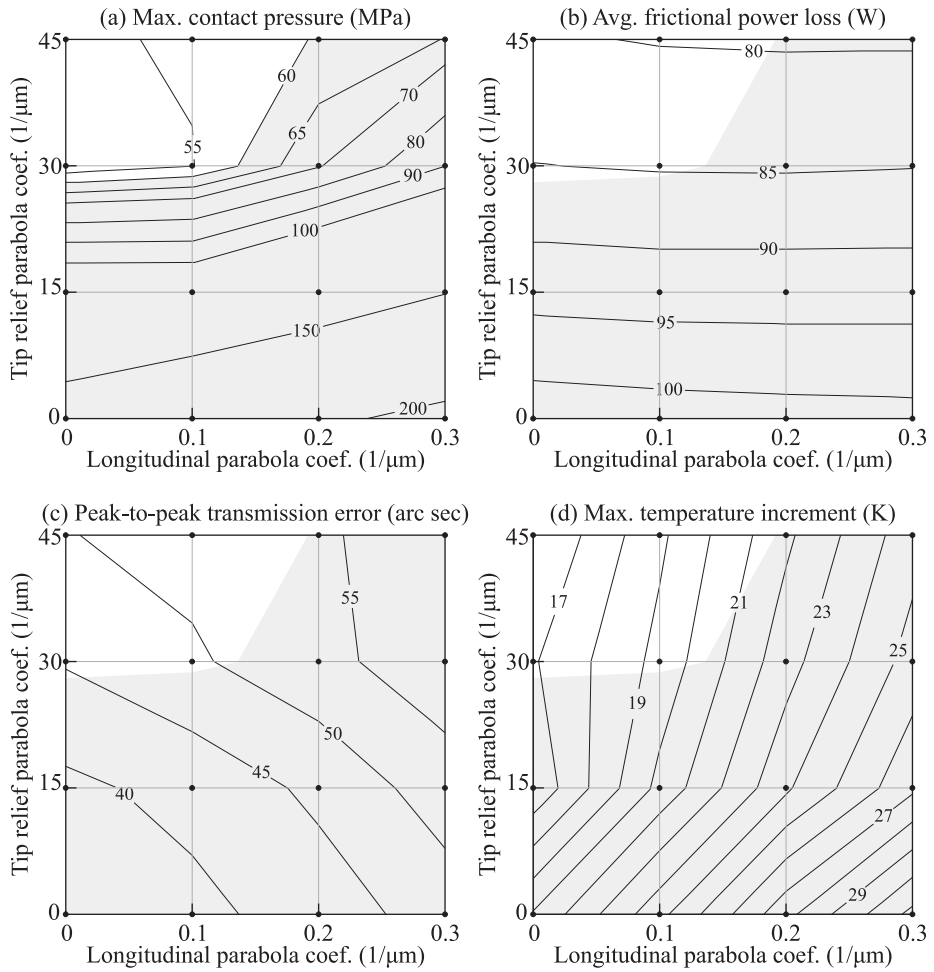

Fig. 10. Results for set B of cases.

Finally, Fig. 9d shows the maximum temperature increment that is produced in the gear tooth. A slight decrease of this temperature is observed as the parabola coefficient for the tip relief is increased. This decrease becomes more significant as the parabola coefficient for the profile crowning is increased.

7.3. Localized bearing contact with a contact path in profile direction

Fig. 10 shows the results obtained from different combinations of longitudinal crowning and tip relief (set B of cases in Table 2). The area shaded in grey indicates those combinations where the maximum contact pressure exceeds 60 *MPa*.

As it can be observed in Fig. 10a, the region of the plot where the maximum contact pressures are below 60 *MPa* is reduced to its left upper part, indicating that in this case large amounts of tip relief are required to avoid the tip contact. When tip contact is avoided, the maximum contact pressure tends to increase as it does the amount of longitudinal crowning, because the curvature of the contact surface is increased.

Regarding the average frictional power loss, Fig. 10b shows that it decreases as the parabola coefficient for the tip relief is increased. In contrast, Fig. 10b reveals that the application of longitudinal crowning has no significant impact on the average frictional power loss. On the other hand, Fig. 10c shows that an increment of the parabola coefficient for the longitudinal crowning implies an increment of the amplitude of the transmission error, which is also increased by the application of tip relief.

Finally, Fig. 10d shows that a slight decrement of the maximum temperature is achieved when the parabola coefficient of the tip relief is increased. On the contrary, and despite the fact that the increment of the parabola coefficient for the longitudinal crowning does not cause an increment of the frictional power loss, it does produce a significant increment of the maximum temperature of the gear.

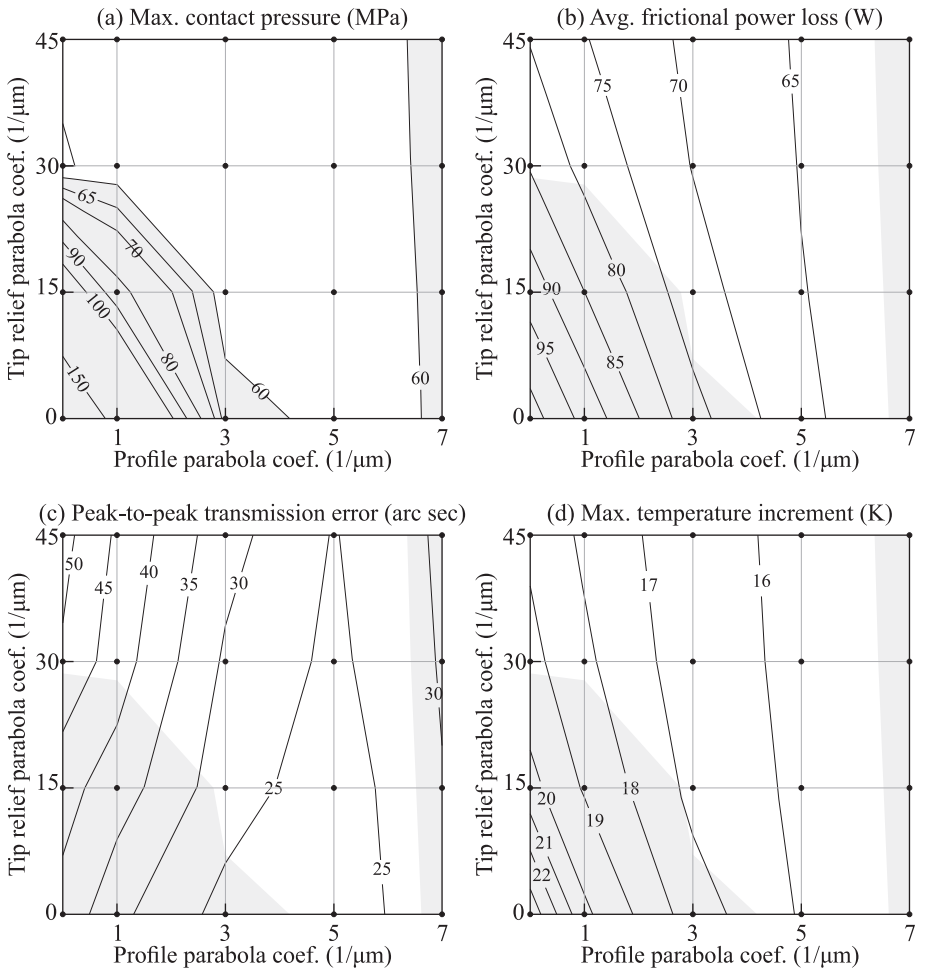

Fig. 11. Results for set C of cases.

7.4. Localized bearing contact with a contact path in a combined direction

Fig. 11 shows the results obtained from different combinations of profile crowning, longitudinal crowning and tip relief (set C of cases in Table 2). The area shaded in grey indicates those combinations where the maximum contact pressure exceeds 60 *MPa*.

The trends that can be observed in Fig. 11 are similar to those illustrated in Fig. 9 for set A of cases. The results show that the average frictional power loss remains unaffected by the application of the longitudinal crowning. In contrast, the maximum contact pressures, peak-to-peak transmission error and maximum operating temperature present higher values than the ones observed in Fig. 9.

7.5. Comparison of selected cases of study

After assessing the impact of different contact pattern designs on the mechanical and thermal behaviors of the transmission, a comparison between the selected cases of study shown in Table 3 is performed in this section. Fig. 12 shows, at the central gear tooth, the contact pressure distribution for the selected cases of study at a certain contact position of the cycle of meshing. The location of the maximum contact pressure within the contact area is marked with a black dot. Furthermore, the reached value of maximum contact pressure is shown. For cases CS02, CS03 and CS04, the contact path is drawn as a polyline that joins those points where the maximum contact pressure is found along the 42 contact positions. Such an illustration allows the contact path direction due to the deformations of the plastic and metal tooth surfaces to be observed. In this way, case CS02 shows a contact path whose direction is practically longitudinal during all the cycle of meshing. A profile-oriented contact path is observed in case CS03 and a contact path in a combined direction is observed in case CS04. For each case, the location of the maximum contact pressure along the contact path is marked with a star.

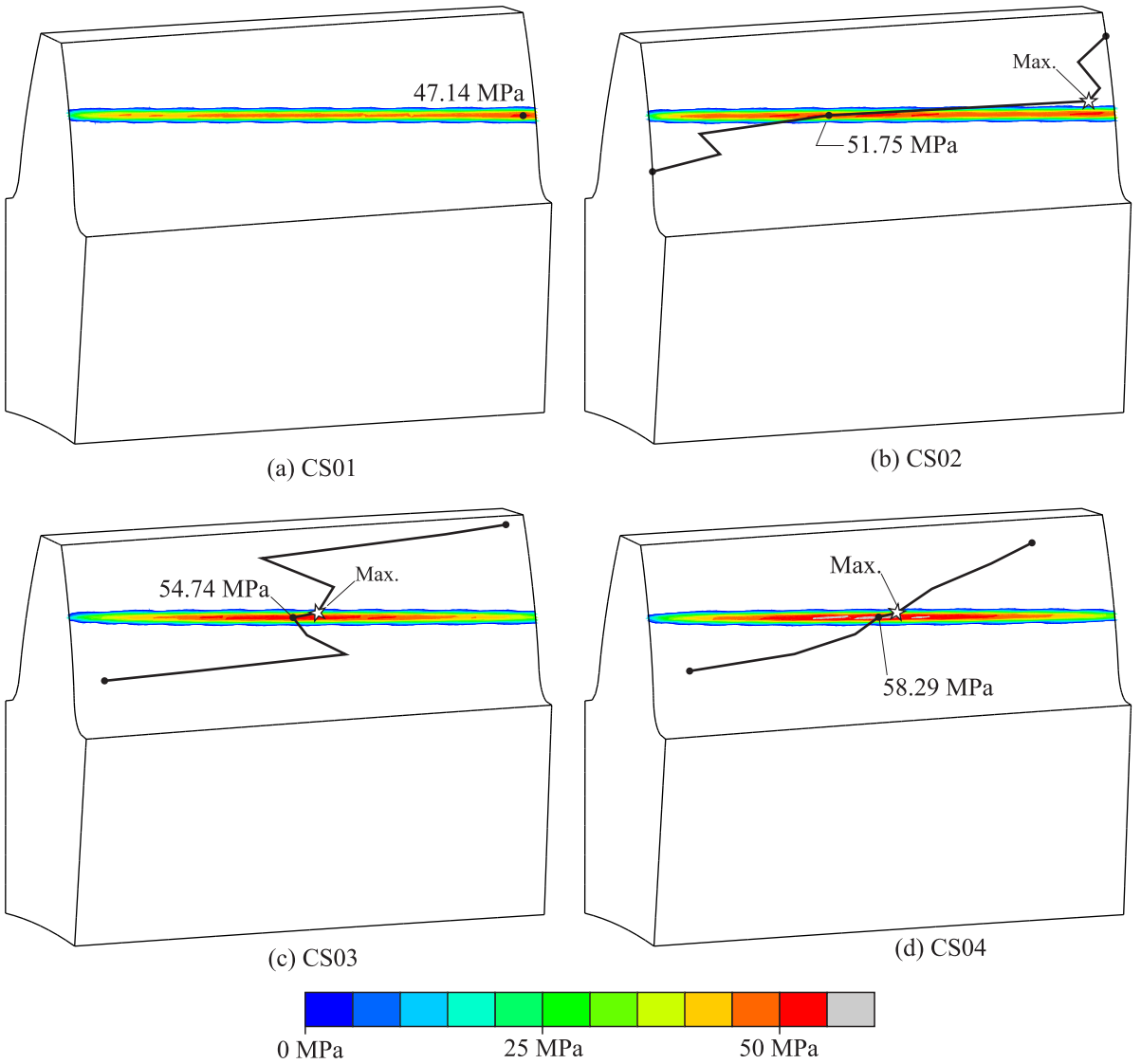

Fig. 12. Contact pressure distribution and contact path under load for selected cases of study.

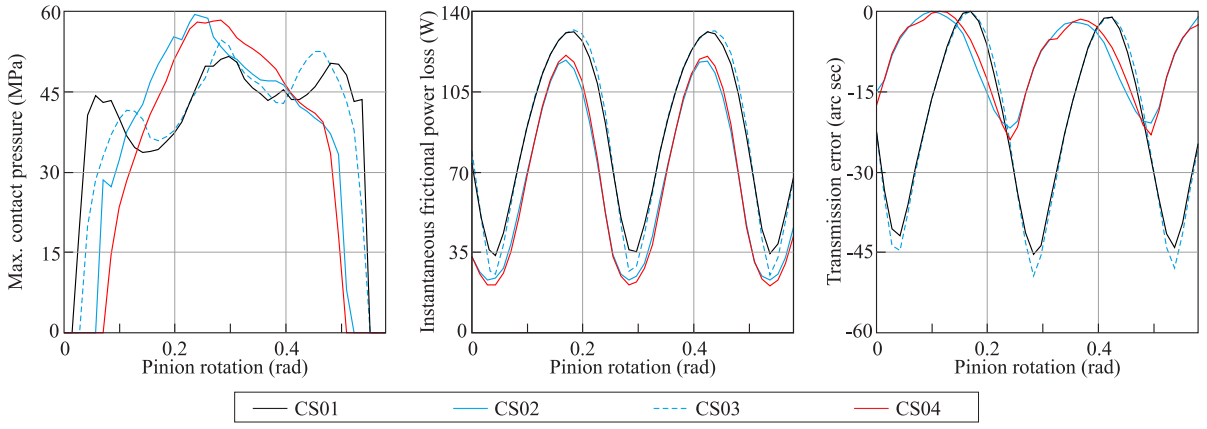

Fig. 13. Results for selected cases of study.

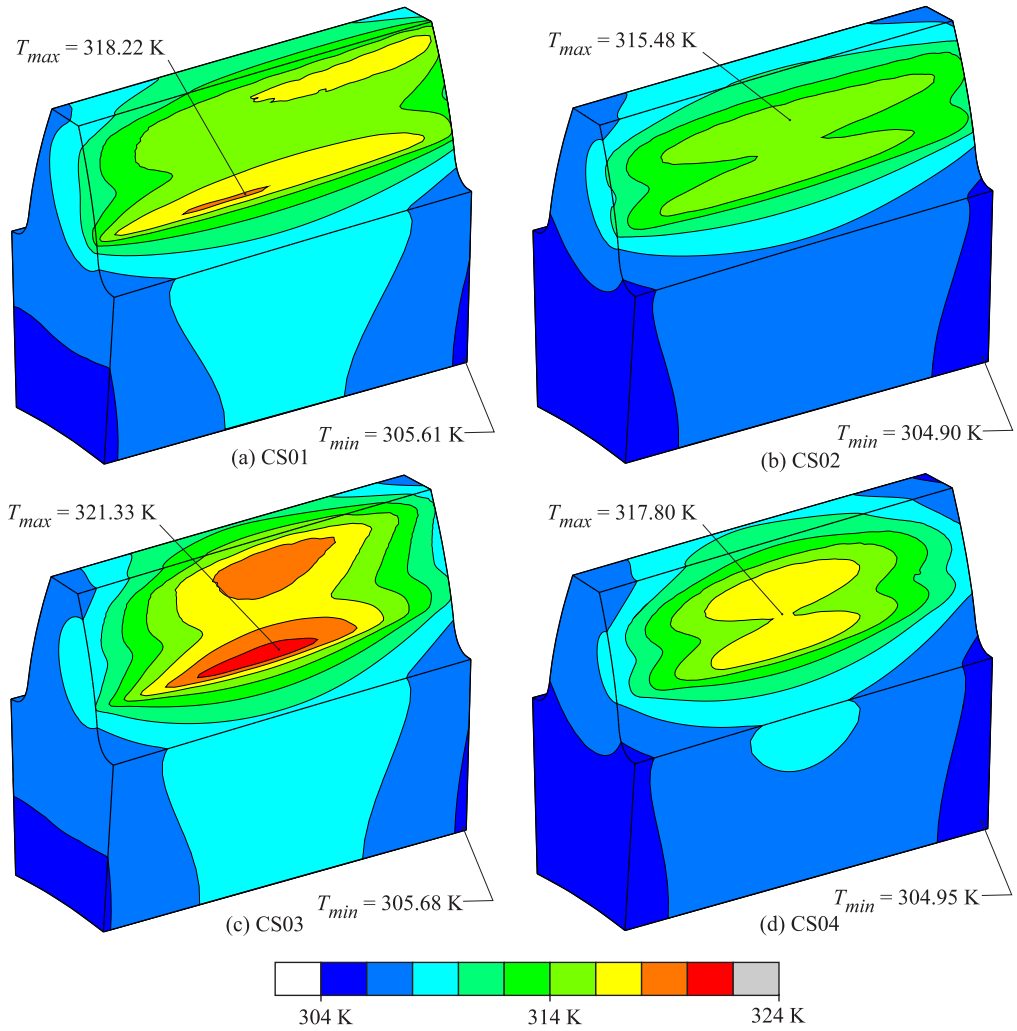

Fig. 14. Temperature field in selected cases of study.

Fig. 13 shows the evolution of the maximum contact pressure, frictional power loss and transmission error for the selected cases of study. It can be observed that the magnitude of the maximum contact pressure is similar for all the selected cases of study, and in all the cases is lower than 60 *MPa*.

The obtained results show that the micro-geometry modifications can bring important reductions of the frictional power loss with respect to the same variable in the standard geometry (discussed in Section 7.1). In those cases where no profile crowning is considered, the application of a tip relief can reduce the average frictional power loss up to 22%. When an additional profile crowning is applied, the average frictional power loss can be reduced more than 40%.

Regarding the transmission error, the obtained results show that the application of the appropriate profile crowning can help reducing the amplitude of the transmission error function. However, if a profile crowning is not applied, the application of a tip relief or a longitudinal crowning may increase the amplitude of the transmission error, with respect to the same variable in the standard geometry.

On the other hand, Fig. 14 shows the temperature field obtained from the thermal analysis of the selected cases of study. The case where the maximum temperature is reached corresponds to CS03, where only a longitudinal crowning is considered, whereas the case where the maximum temperature has a minimum value is CS02, where only a profile crowning is considered. The maximum temperature in case CS04 (double crowning) has a intermediate value between the maximum temperatures reached in cases CS02 and CS03.

To conclude this analysis, the sensitivity of the selected cases of study to a shaft angle error $\Delta\gamma = \pm 0.1$ *deg* is evaluated through the L-TCA of the transmission and illustrated in Fig. 15.

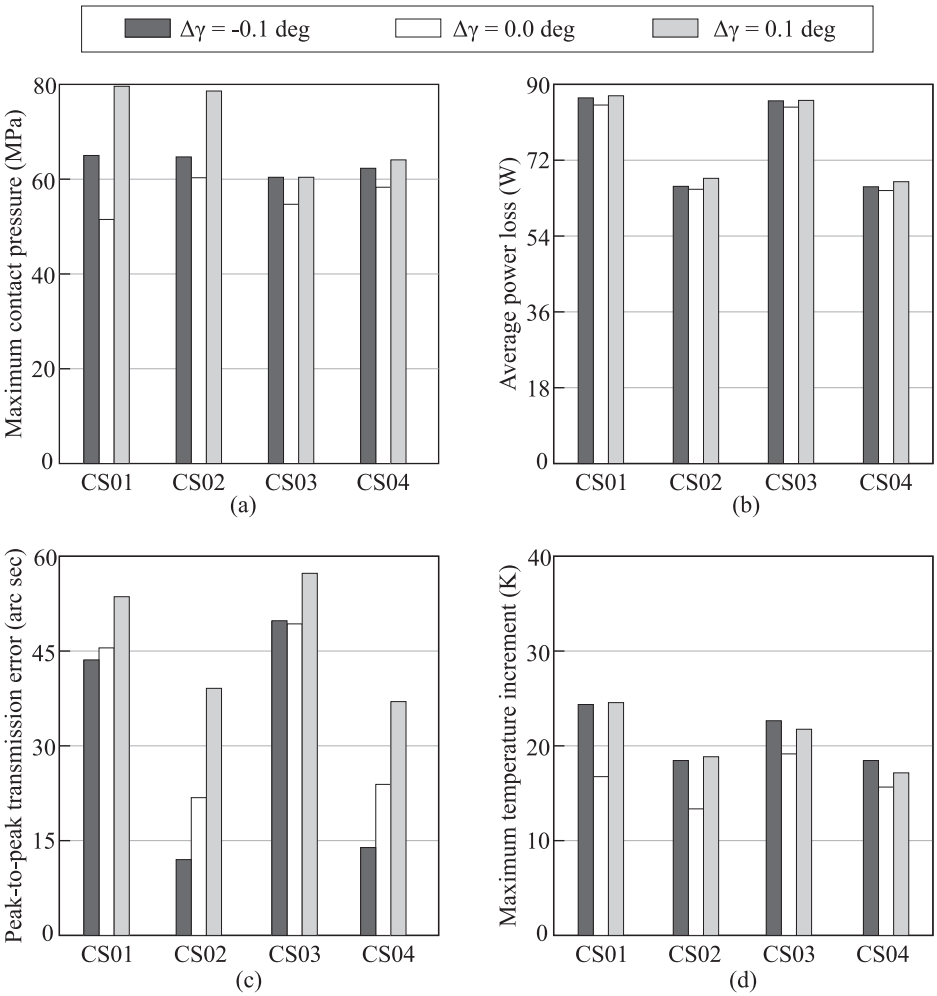

Fig. 15. Variation of results with angular misalignment.

Fig. 15 a shows that the presence of misalignment produces increments of the maximum contact pressure, and these increments are larger when no longitudinal crowning is applied to the pinion tooth surfaces (CS01 and CS02). Fig. 15b shows that the presence of misalignment produces small increments in the average frictional power loss, with a similar magnitude for all the considered cases of study. Fig. 15c shows that the misalignment of the gears produces variations of the amplitude of the transmission error function. When the misalignment is in the positive direction, the amplitude of the transmission error function tends to increase, whereas negative misalignments tend to reduce the amplitude of such a function. Finally, Fig. 15d reveals that the presence of misalignments causes an increase of the maximum temperature increment on the gear teeth. This increment is larger in those cases where no longitudinal crowning is applied.

8. Conclusions

The performed research allows the following conclusions to be drawn:

1. A loaded tooth contact analysis has been applied to a 3D model of a helical gear drive composed of a metal pinion and a plastic gear in order to investigate the effects of the contact pattern design on the contact pressure, the frictional power loss and the peak-to-peak value of loaded transmission errors during the meshing cycle. Furthermore, a steady-state thermal analysis has allowed the temperature increment of the plastic gear to be determined for each contact pattern design.
2. Significance differences are found when comparing a contact pattern design based on a longitudinal direction of the contact path with a design based on a profile direction of the contact path, especially in terms of the frictional power loss, the peak-to-peak transmission error and the temperature increment of the plastic gear, bringing more benefits the first type of design.

3. Regarding the maximum contact pressure, plastic-metal helical gear drives show more sensitivity to misalignments (more specifically, to the crossing shaft angle error) when the contact pattern is not localized or is localized with a longitudinal direction of the contact path.
4. The peak-to-peak value of loaded transmission errors shows as well an important increment when the crossing shaft angle error occurs in the same direction of the helix hand of the pinion. This circumstance occurs for all the considered contact pattern designs, but it is more accentuated in the case of a longitudinally oriented contact path.
5. Furthermore, the increment of the maximum temperature of the gear due to misalignments is more accused when the contact pattern is not localized or is localized with a longitudinal direction of the contact path.
6. The proposed methods of analyses would allow a designer of a plastic-metal helical gear drive to decide the appropriate topology of the pinion and gear tooth surfaces. For the numerical example considered in this work, an optimal profile crowning can bring a reduction in the average frictional power loss, in the amplitude of the loaded function of transmission errors, and in the temperature increment of the plastic gear. The poor response of this type of contact pattern design (based on a longitudinally oriented contact path) when misalignments are present can be amended by considering an additional small amount of longitudinal crowning when designing the contact pattern.

Declaration of Competing Interest

None.

Acknowledgments

The authors express their deep gratitude to the Universitat Jaume I for the financial support of research project ref. UJI-A2019-024.

References

[1] M. Kalin, A. Kupec, The dominant effect of temperature on the fatigue behaviour of polymer gears, Wear 376–377 (2017) 1339–1346, doi:10.1016/j.wear.2017.02.003. 21st International Conference on Wear of Materials
[2] D. Koffi, R. Gauvin, H. Yelle, Heat generation in thermoplastic spur gears, Journal of Mechanical Design, Transactions of the ASME 107 (1) (1985) 31–36, doi:10.1115/1.3258688.
[3] M.G. Wafiuddin, D.I. Daing Mohamad Nafiz, S. Azizul Helmi, S. Januar Parlaungan, A.A. Ismail Ali, A review on failure characteristics of polymer gear, MATEC Web Conf. 90 (2017) 01029, doi:10.1051/matecconf/20179001029.
[4] V. Deutscher Ingenieure, Standard VDI 2736 blatt 2:, thermoplastic gear wheels - cylindrical gears - calculation of the load-carrying capacity, dusseldorf, 2013.
[5] P. Singh, S.A. Singh, An investigation on the thermal and wear behavior of polymer based spur gears, Tribol. Int. 118 (2018) 264–272, doi:10.1016/j.triboint.2017.10.007.
[6] B. Trobentar, S. Glodež, B.Z. Prometheus, B. Zafošnik, Deflection analysis of spur polymer gear teeth, Journal of Multidisciplinary Engineering Science and Technology 2 (2015).
[7] S.A. Singh, S. Yadav, P. Singh, A comparative study for transmission efficiency of abs, pom, and hdpe spur gears, Lecture Notes in Mechanical Engineering (2019) 269–277, doi:10.1007/978-981-13-6469-3_24.
[8] T. Jabbour, G. Asmar, Stress calculation for plastic helical gears under a real transverse contact ratio, Mech. Mach. Theory 44 (12) (2009) 2236–2247, doi:10.1016/j.mechmachtheory.2009.07.003.
[9] C. Hasl, H. Liu, P. Oster, T. Tobie, K. Stahl, Forschungsstelle fuer zahnraeder und getriebebau (gear research centre), method for calculating the tooth root stress of plastic spur gears meshing with steel gears under consideration of deflection-induced load sharing, Mech. Mach. Theory 111 (2017) 152–163, doi:10.1016/j.mechmachtheory.2017.01.015.
[10] S. Evans, P. Keogh, Efficiency and running temperature of a polymer–steel spur gear pair from slip/roll ratio fundamentals, Tribol. Int. 97 (2016) 379–389, doi:10.1016/j.triboint.2016.01.052.
[11] H. Long, A. Lord, D. Gethin, B. Roylance, Operating temperatures of oil-lubricated medium-speed gears: numerical models and experimental results, Proceedings of the Institution of Mechanical Engineers, Part G: Journal of Aerospace Engineering 217 (2) (2003) 87–106, doi:10.1243/095441003765208745.
[12] C. Fernandes, D. Rocha, R. Martins, L. Magalhães, J. Seabra, Finite element method model to predict bulk and flash temperatures on polymer gears, Tribol. Int. 120 (2018) 255–268, doi:10.1016/j.triboint.2017.12.027.
[13] V. Roda-Casanova, F. Sanchez-Marin, A 2d finite element based approach to predict the temperature field in polymer spur gear transmissions, Mech. Mach. Theory 133 (2019) 195–210, doi:10.1016/j.mechmachtheory.2018.11.019.
[14] E. Letzelter, M. Guingand, J.P.D. Vaujany, P. Schlosser, A new experimental approach for measuring thermal behaviour in the case of nylon 6/6 cylindrical gears, Polym. Test. 29 (2010) 1041–1051, doi:10.1016/j.polymertesting.2010.09.002.
[15] Z. Hu, K. Mao, An investigation of misalignment effects on the performance of acetal gears, Tribol. Int. 116 (2017) 394–402, doi:10.1016/j.triboint.2017.07.029.
[16] A. Pogačnik, J. Tavčar, An accelerated multilevel test and design procedure for polymer gears, Mater. Des. 65 (2015) 961–973, doi:10.1016/j.matdes.2014.10.016.
[17] K. Mao, D. Chetwynd, M. Millson, A new method for testing polymer gear wear rate and performance, Polym. Test. 82 (2020) 106323, doi:10.1016/j.polymertesting.2019.106323.
[18] K. Mao, A new approach for polymer composite gear design, Wear 262 (3–4) (2007) 432–441, doi:10.1016/j.wear.2006.06.005.
[19] D. Miler, M. Hoić, Optimisation of cylindrical gear pairs: a review, Mech. Mach. Theory 156 (2021) 104156, doi:10.1016/j.mechmachtheory.2020.104156.
[20] D. Walton, A.B. Cropper, D.J. Weale, P.K. Meuleman, The efficiency and friction of plastic cylindrical gears part 2: influence of tooth geometry, Proceedings of the Institution of Mechanical Engineers, Part J: Journal of Engineering Tribology 2016 (2002) 93–104, doi:10.1243/1350650021543924.
[21] L. Andrei, D. Walton, G. Andrei, E. Mereuta, Influence of a non-standard geometry of plastic gear on sliding velocities, The Annals ff University “Dunarea de Jos” of Galati (2004).
[22] P.K. Meuleman, D. Walton, K.D. Dearn, D.J. Weale, I. Driessen, Minimization of transmission errors in highly loaded plastic gear trains, Proceedings of the Institution of Mechanical Engineers, Part C: Journal of Mechanical Engineering Science 221 (2007) 1117–1129, doi:10.1243/09544062JMES439.
[23] D. Miler, M. Hoić, S. Škec, D. Žeželj, Optimisation of polymer spur gear pairs with experimental validation, Struct. Multidiscip. Optim. 62 (2020) 3271–3285, doi:10.1007/s00158-020-02686-1.

[24] J. Tavčar, B. Černe, J. Duhovnik, D. Zorko, A multicriteria function for polymer gear design optimization, J. Comput. Des. Eng. (2021), doi:10.1093/jcde/qwaa097.
[25] D. Zorko, S. Kulovec, J. Tavčar, J. Duhovnik, Different teeth profile shapes of polymer gears and comparison of their performance, 11, Japan Society of Mechanical Engineers, 2017, doi:10.1299/jamdsm.2017jamdsm0083.
[26] T. Koide, T. Yukawa, S. Takami, A. Ueda, I. Moriwaki, A. Tamura, J. Hongu, Tooth surface temperature and power transmission efficiency of plastic sine-curve gear, Journal of Advanced Mechanical Design, Systems and Manufacturing 11 (6) (2017), doi:10.1299/jamdsm.2017jamdsm0082.
[27] H. Imrek, Performance improvement method for nylon 6 spur gears, Tribol. Int. 42 (2009) 503–510, doi:10.1016/j.triboint.2008.08.011.
[28] H. Düzcükoğlu, R. Yakut, E. Uysal, The use of cooling holes to decrease the amount of thermal damage on a plastic gear tooth, 2010, (????). 10.1007/s11668-010-9398-8
[29] D. Koffi, A. Bravo, L. Toubal, F. Erchiqui, Optimized use of cooling holes to decrease the amount of thermal damage on a plastic gear tooth, Advances in Mechanical Engineering 8 (2016) 1–13, doi:10.1177/1687814016638824.
[30] C.H. Kim, Durability improvement method for plastic spur gears, Tribol. Int. 39 (11) (2006) 1454–1461, doi:10.1016/j.triboint.2006.01.020.
[31] C.M. Fernandes, D.M. Rocha, R.C. Martins, L. Magalhaes, J.H. Seabra, Hybrid polymer gear concepts to improve thermal behavior, J. Tribol. 141 (2019), doi:10.1115/1.4041461.
[32] R.J. Drago, How to design quiet transmissions., Machine Design 52 (28) (1980) 175–181.
[33] F. Litvin, A. Fuentes, I. Gonzalez-Perez, L. Carvenali, K. Kawasaki, R. Handschuh, Modified involute helical gears: computerized design, simulation of meshing and stress analysis, Comput. Methods Appl. Mech. Eng. 192 (33–34) (2003) 3619–3655, doi:10.1016/S0045-7825(03)00367-0.
[34] Z. Chen, M. Zeng, A. Fuentes-Aznar, Geometric design, meshing simulation, and stress analysis of pure rolling cylindrical helical gear drives, Proceedings of the Institution of Mechanical Engineers, Part C: Journal of Mechanical Engineering Science 234 (15) (2020) 3102–3115, doi:10.1177/0954406220912265.
[35] A. Fuentes, H. Nagamoto, F.L. Litvin, I. Gonzalez-Perez, K. Hayasaka, Computerized design of modified helical gears finished by plunge shaving, Comput. Methods Appl. Mech. Eng. 199 (25) (2010) 1677–1690, doi:10.1016/j.cma.2010.01.023.
[36] I. Gonzalez-Perez, A. Fuentes-Aznar, Implementation of a finite element model for gear stress analysis based on tie-surface constraints and its validation through the hertz's theory, Journal of Mechanical Design, Transactions of the ASME 140 (2) (2018), doi:10.1115/1.4038301.
[37] Abaqus theory guide, Dassault Systèmes Simulia Corp, United States, 2015.
[38] M. Karimpour, K.D. Dearn, D. Walton, A kinematic analysis of meshing polymer gear teeth, Proceedings of the Institution of Mechanical Engineers, Part L: Journal of Materials: Design and Applications 224 (3) (2010) 101–115, doi:10.1243/14644207JMDA315.
[39] D. Walton, A.A. Tessema, C.J. Hooke, J.M. Shippen, Load sharing in metallic and non-metallic gears, Proceedings of the Institution of Mechanical Engineers, Part C: Journal of Mechanical Engineering Science 208 (2) (1994) 81–87, doi:10.1243/PIME_PROC_1994_208_104_02.
[40] J. Argyris, A. Fuentes, F. Litvin, Computerized integrated approach for design and stress analysis of spiral bevel gears, Comput. Methods Appl. Mech. Eng. 191 (11–12) (2002) 1057–1095, doi:10.1016/S0045-7825(01)00316-4.
[41] N. Doll, A. Verdesca, E. Bastos, T. Osswald, R. Kleiss, Methodology for quasi-viscoelastic simulation of polymer gears made from peek using ansys, in: Proceedings of the ANTEC, Orlando, FL, USA, 2015.
[42] A.S.S. Takanashi, Uber den temperaturanstieg von zahnen von kunststoffzahnradern (2. bericht): uber die gleichgewichtstemperatur von zahnen von kunststoffzahnrader, Science reports of the Research Institutes, Tohoku University. Ser. A, Physics, chemistry and metallurgy 28 (1) (1979) 103–115.
[43] B. Luo, W. Li, Influence factors on bulk temperature field of gear, Proceedings of the Institution of Mechanical Engineers, Part J: Journal of Engineering Tribology 231 (8) (2017) 953–964, doi:10.1177/1350650116684275.
[44] J. Hartnett, E. Deland, The influence of prandtl number on the heat transfer from rotating nonisothermal disks and cones, J. Heat Transfer 83 (1) (1961) 95–96, doi:10.1115/1.3680479.
[45] R.F. Handschuh, Thermal behavior spiral bevel gears, Vehicle Propulsion Directorate, Army Research Lab. Cleveland, OH., United States, 1995 Ph.D. thesis.
[46] H. Blok, Theoretical study of temperature rise at surfaces of actual contact under oiliness lubricating conditions, Proceedings of General Discussion on Lubrication and Lubricants 2 (1937) 222–235.
[47] G. Erhard, Gear Wheels, in: G. Erhard (Ed.), Designing with Plastics, Hanser, 2006, pp. 411–457, doi:10.3139/9783446412828.011.
[48] V. Deutscher Ingenieure, Standard VDI 2736 blatt 1:, thermoplastic gear wheels - cylindrical gears - materials, material selection, production methods, production tolerance, form design, dusseldorf, 2013.
[49] A. Diez-Ibarbia, A.F. del Rincon, A. de Juan, M. Iglesias, P. Garcia, F. Viadero, Frictional power losses on spur gears with tip reliefs. the load sharing role, Mech. Mach. Theory 112 (2017) 240–254, doi:10.1016/j.mechmachtheory.2017.02.012.